Polarization anisotropy and valence band ordering in semipolar $(11\bar{2}2)$ AlInN/GaN heterostructures

Shawutijiang Sidikejiang,[1,2,*] Philipp Farr,[1,2] Uwe Rossow,[1,2] Heiko Bremers,[1,2] Ferdinand Scholz,[3] and Andreas Hangleiter[1,2,†]

[1]*Institut für Angewandte Physik, Technische Universität Braunschweig, Mendelssohnstrasse 2, 38106 Braunschweig, Germany*

[2]*Laboratory for Emerging Nanometrology, Technische Universität Braunschweig, Langer Kamp 6a, 38106 Braunschweig, Germany*

[3]*Institut für Optoelektronik, Universität Ulm, Albert-Einstein-Allee 45, 89081 Ulm, Germany*

(Received 27 August 2022; accepted 23 December 2022; published 5 January 2023)

Semipolar $(11\bar{2}2)$ AlInN/GaN heterostructures on GaN templates were studied using photoluminescence (PL) spectroscopy both at 15 K and at room temperature. The polarization-resolved PL measurements revealed a dominant polarization along the $[11\bar{2}\bar{3}]$ c' and a weaker signal along the $[1\bar{1}00]$ m-direction, i.e., the two in-plane directions of the semipolar $(11\bar{2}2)$ growth plane. We observed slightly different polarization degrees of 0.34 ± 0.01, 0.25 ± 0.02, and 0.20 ± 0.01 at room temperature, respectively, depending on the degree of strain relaxation in the $[1\bar{1}00]$ direction. From a theoretical model based on a $\mathbf{k} \cdot \mathbf{p}$ calculation, we find that the transition from the conduction band (CB) to the uppermost valence band (VB) is C for AlInN similar to AlN, followed by the transition A from the CB to the second VB, for a wide range of compositions. Thus, the in-plane transition matrix elements from the CB to the two topmost VBs near the Γ point of the *Brillouin* zone are dominated by $M_{[11\bar{2}\bar{3}]}$ for the C transition and by $M_{[1\bar{1}00]}$ for the A transition. For the samples under consideration with an energy splitting of about 18 ± 1 meV, there is sizable thermal occupation of the second VB at room temperature, reasonably explaining the experimental results. The results show that AlInN possesses a band structure similar to AlN, which might explain the strong Stokes shift and the large variation in the band-gap values reported previously.

DOI: 10.1103/PhysRevB.107.045202

I. INTRODUCTION

AlInN/GaN heterostructures have drawn considerable attention recently as promising candidates for high-power electronics [1,2] as well as for improving the performance of optoelectronic devices [3,4]. The use of AlInN structures is of particular interest, since it can be grown lattice-matched to GaN on a c-plane with an indium composition of approximately 18% according to Vegard's rule [5]. For non- and semipolar crystal orientations, AlInN can be grown lattice-matched only in one of the in-plane directions of non-c-polar growth planes due to the difference in a/c ratios of GaN and AlInN. Buss *et al.* [6,7] have recently demonstrated an intentional one-directional relaxation of the AlInN lattice in a non-lattice-matched direction for semipolar AlInN structures by controlling the indium composition and thickness. Application of AlInN as a strain-reducing buffer layer in semipolar green-emitting GaInN/GaN quantum wells (QWs) has recently been successfully demonstrated [8]. Although the structural properties of AlInN have been studied extensively, fundamental optical properties of the AlInN, such as the band gap and bowing parameter, are not well known. Moreover, there is significant scattering in the band-gap energy and the bowing parameter reported previously [9–14]. The large span of the reported values may be attributed to a number of factors, including poor sample quality, the details of the experiments, and more likely, a lack of knowledge about the polarization selection rules that are associated with the valence band ordering near the Γ point ($k = 0$) in the *Brillouin* zone for AlInN.

The valence band (VB) maximum of wurtzite materials is split into three bands of symmetry Γ_9^V, Γ_7^V, and Γ_{7-}^V [15], the splitting being described by the spin-orbit interaction Δ_{so} and the crystal-field splitting Δ_{cr}. Usually, the ordering of valence bands is determined by the sign of Δ_{cr}, which is positive in the case of GaN (where the Γ_9^V band is the uppermost valence band). For AlN, Δ_{cr} is negative with a large value of around -217 meV [15,16], thus the valence bands have Γ_{7-}^V, Γ_9^V, and Γ_7^V symmetries with the Γ_{7-}^V band being the uppermost one. It is worth mentioning that the interband transitions between the conduction band (CB) and these bands are usually labeled as A (transition from CB to Γ_9^V), B (transition from CB to Γ_7^V), and C (transition from CB to Γ_{7-}^V) in the order of increasing transition energy in the case of GaN [17–19]. For the selection rules for electric dipole transitions in AlN, the C interband transition is allowed for an electric field parallel to the c-axis ($E \parallel c$) but strictly forbidden for polarization perpendicular to the c-axis ($E \perp c$). The opposite applies for the A and B transitions, thus only $E \perp c$ is allowed. As a result, the C transition is strongly polarized for $E \parallel c$. This indicates that the C transition, which determines the band gap energy, is hardly detectable for optical characterization with light normal to the c-plane such as absorption, transmission, and reflectance. However, the situation is expected to be quite different for non- or semipolar structures. Unlike polar c-plane

*s.sidikejiang@tu-braunschweig.de
†a.hangleiter@tu-braunschweig.de

TABLE I. Overview of the samples under investigation, with the thickness (d_{AlInN}), indium composition (x_{In}), as well as the degree of strain relaxation in the m-direction (R_{m}). The emission energy at 300 K ($E_{300\ \mathrm{K}}$), the full width at half-maximum at 300 K ($w_{300\ \mathrm{K}}$), and the polarization degrees both at 300 K ($\rho_{300\ \mathrm{K}}$) and 15 K ($\rho_{15\ \mathrm{K}}$) are listed.

Sample	d_{AlInN} (nm)	x_{In} (%)	R_{m} (%)	$E_{300\ \mathrm{K}}$ (eV)	$w_{300\ \mathrm{K}}$ (meV)	$\rho_{300\ \mathrm{K}}$	$\rho_{15\ \mathrm{K}}$
S1	≈290	26.9 ± 0.3	31 ± 2	3.12	304	0.34 ± 0.01	0.48 ± 0.01
S2	≈140	28.5 ± 0.2	39 ± 10	3.05	370	0.25 ± 0.02	
S3	≈400	28.8 ± 0.3	94 ± 6	2.99	303	0.20 ± 0.01	0.22 ± 0.01

structures, non- and semipolar planes have reduced crystal symmetries, which give rise to optical polarization anisotropy. Therefore, access to this polarization anisotropy by growing AlN-based ternary compounds on non-c-plane orientations opens up a new way to gain a better understanding of the fundamental optical properties of those structures. So far there have been a number of publications [9–14] reporting the band-gap energy and bowing parameters of AlInN structures. The strong dependence of excitonic transitions on the polarization selection rules is often neglected, which might be a reason for the large variation of those reported values. To our knowledge, no attempt has been made to study the polarization anisotropy of non-c-plane AlInN layers. Recently, however, Laskar *et al.* [20] reported the successful growth of a-plane $(11\bar{2}0)$ AlInN/GaN epitaxial layers, and a strong polarization anisotropy with a dominant polarization along the [0001] ($E \parallel c$) is observed. Although the luminescence properties of m-plane AlInN grown on free-standing GaN templates have been investigated under steady-state conditions using both optical reflectance and cathodoluminescence (CL) measurements, the m-plane AlInN epilayers do not show distinguishable polarization anisotropy in the measured spectra, which gives rise to concerns regarding the origin of the emission lines observed in AlInN layers by Chichibu *et al.* [13].

In this present work, we analyze the polarization anisotropy of semipolar $(11\bar{2}2)$ AlInN/GaN heterostructures grown on GaN templates using polarization-resolved photoluminescence (PL) spectroscopy. Polarization-dependent PL measurements reveal a dominant polarization along the $[11\bar{2}\bar{3}]$ direction and a weaker signal along the $[1\bar{1}00]$ direction. We observe a gradual decrease of the polarization degree with increasing strain relaxation along $[1\bar{1}00]$ in AlInN layers. The VB structure and the in-plane transition matrix elements were calculated by a theoretical model based on a $\mathbf{k} \cdot \mathbf{p}$ calculation. The simulation results show that AlInN layers possess a VB ordering similar to AlN, where the C transition from the CB to the uppermost valence Γ_{7-}^{V} is strongly polarized along the $[11\bar{2}\bar{3}](E \parallel c')$, followed by the transition A from the CB to the second valence Γ_{9}^{V} band, which shows a dominant polarization along the m-direction ($E \perp c'$), and this holds for a wide range of indium contents. Our model predicts a small energy difference ΔE of about 23 meV between the two topmost VBs for the samples under investigation, which results in a sizable thermal population of the second Γ_{9}^{V} band at room temperature. This could reasonably explain the experimentally observed energy difference ΔE of about 18 ± 1 meV at 300 K between the two in-plane polarization components. In addition, our understanding of the AlInN VB structure may be helpful to explain some scattering of experimental data for AlInN layers reported earlier, such as a large variation of the band gap and bowing parameters.

II. EXPERIMENTAL DETAILS

The samples under investigation (labeled S1, S2, and S3) have been prepared using low-pressure metalorganic vapor phase epitaxy (MOVPE) in a commercial Aixtron AIX200RF reactor. High-resolution x-ray diffraction (XRD) has been employed for structural characterization. The AlInN/GaN structures are grown on semipolar $(11\bar{2}2)$ oriented GaN templates on a prestructured r-plane sapphire substrate. The details on the template growth can be found elsewhere [21]. The growth on the template starts with a GaN buffer layer of about 100 nm thickness, followed by the AlInN layer. The AlInN layers were grown for 70–200 min at temperatures between 760 and 810 °C, resulting in layer thicknesses of 140–400 nm and an indium concentration of about 28%. $(11\bar{2}2)$ AlInN can be grown lattice-matched to GaN along the $[11\bar{2}\bar{3}]$ direction at an indium composition of around 26%, and it is compressively strained ($\epsilon_m \approx -1.04\%$) along $[1\bar{1}00]$. By controlling the AlInN layer thickness, an intentional one-directional strain relaxation of the AlInN lattice along the m-direction has been realized [6], and an enhancement of indium incorporation in QWs has been observed with increasing strain relaxation in the AlInN layers. With an indium content of 18%, on the other hand, lattice-matching in $[1\bar{1}00]$ leaves the AlInN lattice under tensile strain ($\epsilon_{c'} \approx +1.03\%$) along $[11\bar{2}\bar{3}]$, and the in-plane c'-lattice parameter would be forced to take even a smaller value due to strain relaxation, thus leading to even larger lattice-mismatch between the AlInN and the underlying GaN template. For further details regarding the strain relaxation in AlInN layers, see Refs. [6,7]. As the initial aim of growing the semipolar $(11\bar{2}2)$ AlInN/GaN layers was to achieve lattice-matching along the c'-direction, the indium concentrations in AlInN layers in the present study are limited to around 28%, as confirmed by XRD. A summary of the structural analysis and of the PL characteristics of samples is given in Table I.

The PL measurements were carried out using a cw frequency-doubled diode-pumped 532 nm laser with an excitation wavelength of 266 nm and an argon-ion laser with a 335 nm excitation wavelength both at 15 and 300 K. For PL measurements, the laser beam is focused to a spot size of about 100 μm on the sample, and the PL signal is collected from the surface-normal with a lens with a numerical aperture (NA) of 0.35. This NA corresponds to a collection angle of 21° in air (8° in AlInN) around the optical axis. The polarization dependence of the PL signal is measured by the combination

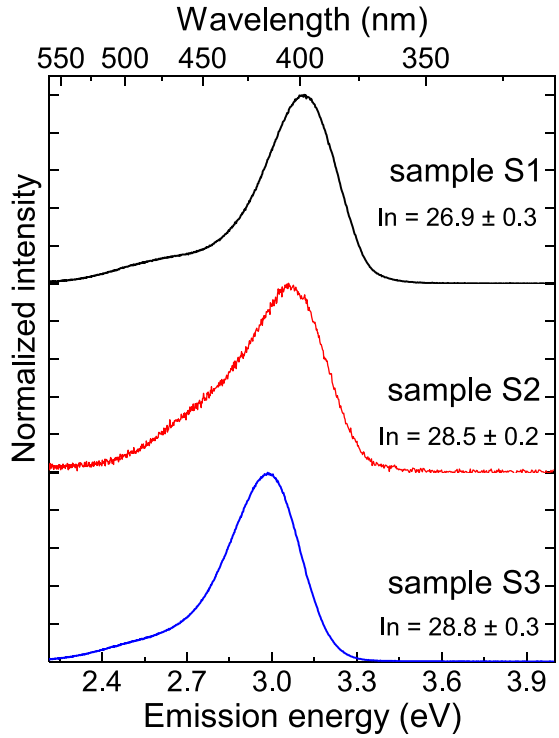

FIG. 1. Photoluminescence spectra measured at 300 K with an excitation wavelength of 266 nm for semipolar $(11\bar{2}2)$ AlInN layers (S1, S2, and S3). Each spectrum is normalized to the respective maximum peak intensity, and the spectra are shifted vertically for clarity.

of a Glan-Thompson polarizer at a fixed angle and a half-wave plate ($\lambda/2$) to rotate the polarization. In addition, we observe a dependence of the polarization degree on the radial distance from the cryostat vacuum window center, e.g., generally a distortion of polarization is induced by stress-induced birefringence in the vacuum window [22].

III. EXPERIMENTAL RESULTS

Figure 1 shows the PL spectra of the AlInN epitaxial layers with indium compositions of $26.9 \pm 0.3\%$, $28.5 \pm 0.3\%$, and $28.8 \pm 0.3\%$ for samples S1, S2, and S3, respectively. The spectra were measured at 300 K with laser excitation at 266 nm. Generally, a broadband emission is commonly observed for all three samples with peak emissions appearing at 3.12, 3.05, and 2.99 eV for samples S1, S2, and S3. A clear redshift of the main emission peak is observed as indium composition increases, which is an expected response of the band-gap energy with increasing indium content. Apart from sample S2, the linewidths of samples S1 and S3 are comparable to the previously reported values of about 290 meV measured at 300 K [11,12]; see Table I. In addition, the absence of the band-edge emission of the underlying GaN layer is evidence that the penetration depth of the 266 nm laser line is likely limited only to the AlInN layers. Thus, this provides additional evidence that the broadband emission can be assigned to the band-to-band transition from the AlInN epilayers.

Unlike the c-plane, due to the broken hexagonal radial symmetry around the c-axis for non-c-plane orientations, the emitted light from structures grown on these planes exhibits a polarization anisotropy, which can be accessed by polarization-resolved PL measurements. Figure 2 shows the polarization anisotropy of the semipolar $(11\bar{2}2)$ AlInN epilayer (sample S3) both at 15 and 300 K together with the dependence of the integrated PL intensities on the polarization angle ϕ in polar plots. As can be clearly seen in Fig. 2(a), a strong PL signal is observed with polarization perpendicular to the $[1\bar{1}00]$, i.e., along the $[11\bar{2}\bar{3}]$ direction, and a weaker PL intensity is observed along the $[1\bar{1}00]$ direction. This provides strong evidence that the luminescence is polarized strongly along the $[11\bar{2}\bar{3}]$ direction for semipolar $(11\bar{2}2)$ AlInN layers. This can be intuitively understood by taking the properties of the $(11\bar{2}2)$ growth plane into consideration, since the growth plane is constituted by $[1\bar{1}00]$ m and $[11\bar{2}\bar{3}]c'$ directions, and the latter corresponds to the projection of the c-axis onto the plane of growth. Generally, the polarization in a semipolar plane is mainly determined by the tilt of the c-axis with respect to the growth plane. Thus, the observed large polarization along the $[11\bar{2}\bar{3}]$ direction is, in turn, equivalent to a strong polarization along the c-axis in the usual (0001) plane case, i.e., the E-field parallel to the c-axis ($E \parallel c$). Furthermore, a comparison of the polarization anisotropies of a semipolar $(11\bar{2}2)$ AlInN/GaN epilayer and a semipolar $(11\bar{2}2)$ GaInN/GaN quantum well with an indium content of about 19% reveals that the polarization in AlInN/GaN is just the opposite case to the GaInN/GaN structure, where the dominant polarization is along $[1\bar{1}00]$ (not shown here). This corresponds to the E-field perpendicular to the c-axis ($E \perp c$), which is consistent with the results reported in the literature [23,24]. Nonetheless, this does not hold true for GaInN/GaN structures with indium compositions greater than ∼30%, where the dominant polarization was observed to switch from the $[1\bar{1}00]$ to the $[11\bar{2}\bar{3}]$ direction. The effects of quantum confinement and in-plane strain are commonly assigned as the cause of the polarization changes [25–27]. From the experimental results, we can derive a solid conclusion that AlInN layers possess a valence band structure similar to that of AlN. Therefore, the dominant polarization ($E \parallel c'$) corresponds to an interband transition from the CB to the topmost valence band Γ_{7-}^{V}, and the weaker one ($E \parallel m$) results from a transition between the CB and the second uppermost Γ_{9}^{V} band, and followed by the transition B.

To gain further insight into the polarization properties, the normalized integrated PL intensity is plotted against the polarization angle ϕ with respect to the $[1\bar{1}00]$ direction, as shown in Figs. 2(c) and 2(d). The general polarization property of linearly polarized light can be described by Malus' law [28], which is given as

$$I(\phi) = I_{\perp[1\bar{1}00]} \sin^2(\phi) + I_{\parallel[1\bar{1}00]} \cos^2(\phi), \qquad (1)$$

where $I_{\perp[1\bar{1}00]}$ and $I_{\parallel[1\bar{1}00]}$ denote the integrated intensities of the emitted light polarized perpendicular and parallel to the $[1\bar{1}00]$ direction, respectively. It can be easily seen from the polar plots in Figs. 2(c) and 2(d) that the model reproduces very well the measured data points, indicating very good agreement between the theory and experimental data measured both at 15 and 300 K. By fitting the angular-dependent

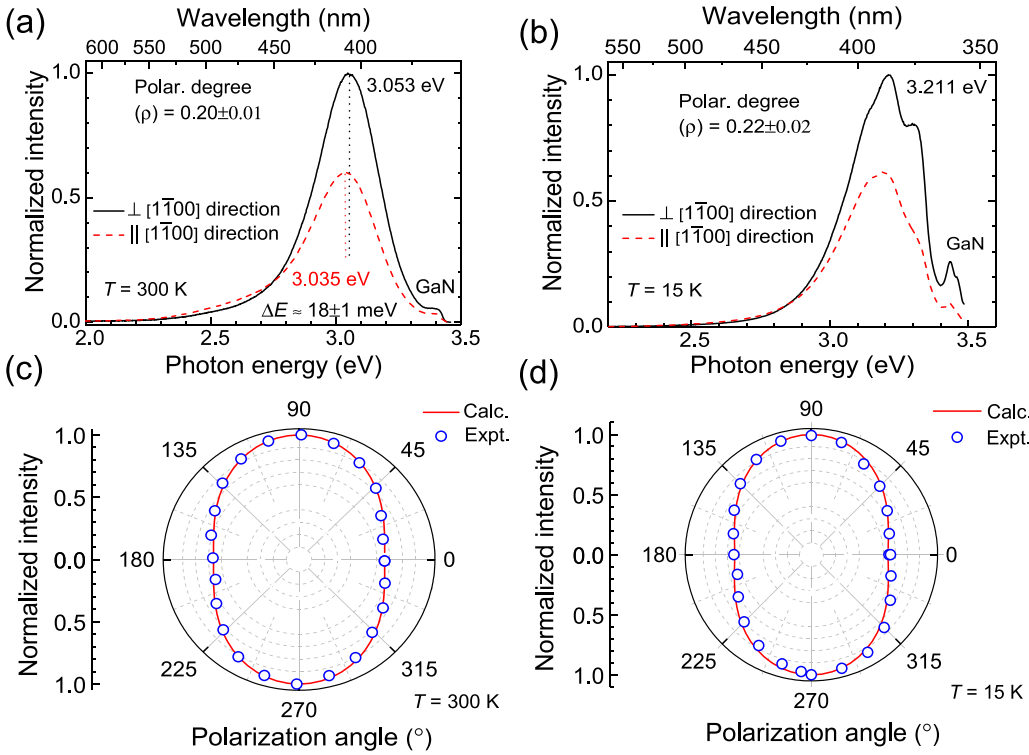

FIG. 2. (a), (b) Normalized PL spectra of the semipolar (11$\bar{2}$2) AlInN layer (sample S3) for the collected light polarized parallel (dashed line) and perpendicular (solid line) to the [1$\bar{1}$00] *m*-direction of the (11$\bar{2}$2) plane both at 15 and 300 K. PL was excited using the 335 nm line of an argon-ion laser in the measurements in this case. The band-edge emission of the underlying GaN appears at around 3.4 eV. Note that the contribution of the GaN band emission is deducted from the total integrated PL intensity in the analysis. An energy separation of about $\Delta E \approx 18 \pm 1$ meV is observed between the two in-plane polarization components for the sample S3 at 300 K. In contrast, the low-temperature spectra were modulated by the Fabry-Pérot fringes, which makes it difficult to determine the actual energy separation, but there is a clear blueshift of the emission energy with decreasing temperature. (c), (d) Polar plots of the normalized integrated PL signal as a function of the in-plane polarization angle ϕ of the emitted light with respect to the the *m*-direction both at 15 and 300 K. The open circles represent the integrated measured PL intensities, and the red solid lines denote calculated curves given in Eq. (1).

PL intensities, a polarization ratio of 0.20 ± 0.01 is estimated for sample S3 at 300 K. Here the polarization degree is defined as $\rho = (I_{\perp[1\bar{1}00]} - I_{\parallel[1\bar{1}00]})/(I_{\perp[1\bar{1}00]} + I_{\parallel[1\bar{1}00]})$. It is interesting to note that an increase of the polarization degrees is observed for samples S1 and S2 as being 0.34 ± 0.01 and 0.25 ± 0.02, respectively; see Table I. At first glance, this can be explained qualitatively by considering the strain relaxation in semipolar (11$\bar{2}$2) AlInN/GaN layers. As demonstrated in earlier work [6], the in-plane lattice parameters of the AlInN layers in the [1$\bar{1}$00] direction take somewhat larger lattice parameter values with respect to the underlying GaN template when lattice-matching is intended in the [11$\bar{2}\bar{3}$] direction with an indium composition of about 28%. The strain relaxation becomes more significant when the AlInN layer thickness increases. Accordingly, $(94 \pm 6)\%$ strain relaxation in the AlInN layer is estimated for sample S3 with a layer thickness of around 400 nm, while the AlInN layers in samples S1 and S2 exhibit partial relaxation in the [1$\bar{1}$00] direction with relaxation degrees of $(31 \pm 2)\%$ and $(39 \pm 10)\%$, respectively; see Table I. The optical polarization anisotropy directly reflects the valence band ordering of emitting structures. Thus the polarization degree could be affected by the change in the band character of the two topmost VBs, which might be caused by the band crossing due to strain. Anisotropic in-plane strain as well as shear strain in the (11$\bar{2}$2) plane have been shown to have a significant impact on the modification of the VB through deformation potentials [27,29]. Yan *et al.* [27] found that the relative energy separation between the two topmost VBs becomes smaller when strain relaxation in the [1$\bar{1}$00] direction is larger than that along the [$\bar{1}\bar{1}$23] direction in a semipolar (11$\bar{2}$2) GaInN layer, which corresponds to an increase of strain along [11$\bar{2}\bar{3}$]. Thus, one could expect a decrease of the polarization degree with increasing in-plane strain in the [$\bar{1}\bar{1}$23] direction. A theoretical model based on multiband effective-mass theory predicted a similar trend of a decreasing polarization degree when the strain relaxation in the [1$\bar{1}$00] direction becomes larger in semipolar (11$\bar{2}$2) GaInN/GaN quantum wells [30]. So it is not surprising to see the decrease of the polarization degree with increasing strain relaxation in the [11$\bar{2}\bar{3}$] direction due to the modification of the VB structure induced by anisotropic strain.

In addition, the emitted light polarized parallel to [1$\bar{1}$00] shows an energy of about $\Delta E \approx 18 \pm 1$ meV higher than that of the polarization perpendicular to [1$\bar{1}$00] at 300 K. The effective energy difference depends essentially on the anisotropic in-plane strain in the semipolar growth plane, which might be subject to the choice of the band parameters, e.g., deformation potentials. As demonstrated in the following, the observed energy splitting of about $\Delta E \approx 18 \pm 1$ meV is explained reasonably well with a theoretical model based

on $\mathbf{k}\cdot\mathbf{p}$ perturbation theory. The model predicts an energy separation of 23 meV between the two topmost VBs for S3, which results in a sizable thermal population of the second topmost valence band at 300 K. In contrast, the other two samples (S1 and S2) do not show energy splittings between the two in-plane polarization components in the measurement, despite the fact that the model predicts energy splittings of about 33 and 27 meV between the two uppermost VBs for samples S1 and S2, respectively. This might be due to the large widths of the observed PL bands, and their energy splittings are likely buried by the large linewidth.

The low-temperature PL spectra of the sample S3 for the two polarization directions are shown in Fig. 2(b). It can easily be seen that the low-temperature polarization anisotropy is similar to that measured at room temperature [Fig. 2(a)], exhibiting strong polarization along $[11\bar{2}\bar{3}]$. Additionally, the mean emission peak shifts to higher energy at low temperature, which is a typical behavior due to the temperature dependence of the band gap. However, the PL spectra show features of multiple peaks around the main emission line centered at 3.211 eV. This is likely due to the Fabry-Pérot (FP) cavity formed by the GaN/air and GaN/sapphire interfaces. A model consisting of a Gaussian function together with three phonon replicas and a FP filter function reasonably represents the observed PL spectra (not shown here), and it yields a GaN thickness of about 3 μm in agreement with the intended thickness of GaN during template preparation [21]. The polarization degrees are found to increase slightly at low temperature, which can be explained in terms of the thermal distribution of holes in the higher-energy bands at elevated temperature. In the low-temperature limit, on the other hand, there is almost no thermal population of holes in the second uppermost valence Γ_9^V band, which results in a higher degree of polarization.

IV. VALENCE BAND ORDERING AND STRAIN RELAXATION

To further investigate the polarization properties of semipolar AlInN/GaN structures in a quantitative manner, the $\mathbf{k}\cdot\mathbf{p}$ perturbation approach proposed by Bir and Pikus [31] was employed to theoretically estimate the optical properties of AlInN near the Γ point of the Brillouin zone. Due to the relatively large band gap of AlInN, the interaction between the conduction and valence bands can be treated as a weak perturbation, which allows us to express explicitly the VB Hamiltonian (H_v) via a 6×6 matrix [29]:

$$H_\mathrm{v}=\begin{bmatrix} F & -K^* & -H^* & 0 & 0 & 0\\ -K & G & H & 0 & 0 & \Delta\\ -H & H^* & \Lambda & 0 & \Delta & 0\\ 0 & 0 & 0 & F & -K & H\\ 0 & 0 & \Delta & -K^* & G & -H^*\\ 0 & \Delta & 0 & H^* & -H & \Lambda \end{bmatrix}, \quad (2)$$

where

$$F=\Delta_1+\Delta_2+\Lambda+\Theta, \qquad G=\Delta_1-\Delta_2+\Lambda+\Theta,$$

$$\Lambda=\frac{\hbar^2}{2m_0}\left[A_1k_\mathrm{z}^2+A_2\left(k_\mathrm{x}^2+k_\mathrm{y}^2\right)\right]+D_1\varepsilon_{zz}+D_2(\varepsilon_{xx}+\varepsilon_{yy}),$$

$$\Theta=\frac{\hbar^2}{2m_0}\left[A_3k_\mathrm{z}^2+A_4\left(k_\mathrm{x}^2+k_\mathrm{y}^2\right)\right]+D_3\varepsilon_{zz}+D_4(\varepsilon_{xx}+\varepsilon_{yy}),$$

$$K=\frac{\hbar^2}{2m_0}A_5(k_\mathrm{x}+ik_\mathrm{y})^2+D_5(\varepsilon_{xx}-\varepsilon_{yy}),$$

$$H=\frac{\hbar^2}{2m_0}A_6(k_\mathrm{x}+ik_\mathrm{y})k_\mathrm{z}+D_6\varepsilon_{zx},$$

$$\Delta=\frac{\sqrt{2}}{3}\Delta_\mathrm{so}. \quad (3)$$

The Hamiltonian includes the spin-orbit ($\Delta_1=\Delta_\mathrm{cr}$) and crystal-field splitting ($\Delta_2=\frac{1}{3}\Delta_\mathrm{so}$) energies, the deformation potentials D_i ($i=1,\ldots,6$), which describe the shift of the valence band maxima due to strain, and the inverse effective-mass parameters A_i ($i=1,\ldots,6$) as well as the wave vectors and strain components $\mathbf{k}_\mathrm{i}$, $\varepsilon_\mathrm{ij}\in\{x,y,z\}$. Almost all band parameters are linearly interpolated between AlN and InN band parameters proposed by Vurgaftman *et al.* [16]. The basis functions for the H_v are defined as follows:

$$|u_1\rangle=-\frac{1}{\sqrt{2}}|(X+iY)\uparrow\rangle, \quad |u_2\rangle=-\frac{1}{\sqrt{2}}|(X-iY)\uparrow\rangle,$$

$$|u_3\rangle=|(Z)\uparrow\rangle, \quad |u_4\rangle=-\frac{1}{\sqrt{2}}|(X-iY)\downarrow\rangle,$$

$$|u_5\rangle=-\frac{1}{\sqrt{2}}|(X+iY)\downarrow\rangle, \quad |u_6\rangle=|(Z)\downarrow\rangle, \quad (4)$$

Here $|X\rangle$, $|Y\rangle$, and $|Z\rangle$ have the symmetry of the atomic p_x-, p_y-, and p_z-orbital wave functions. $|\uparrow\rangle$ and $|\downarrow\rangle$ denote the wave functions with spin-up and spin-down states, respectively. These basis functions represent the hole wave functions in the valence bands, and their linear combinations will be the solutions to the Schrödinger equation, e.g., the eigenfunctions of the Hamiltonian in Eq. (2). This can be written as

$$|\Psi_\mathrm{v}(\mathbf{k})\rangle=\sum_{\mathrm{i}=1}^{6}b_\mathrm{i}(\mathbf{k})|u_i\rangle. \quad (5)$$

Using diagonalization algorithms, the eigenfunctions and energies of the Hamiltonian can be found, which yields three distinct VB maxima energies and the prefactors b_i ($\mathrm{i}=1,2,\ldots,6$) for the basis functions defined in Eq. (4).

The Hamiltonian for the strain-dependent modification of the conduction band is described by a 2×2 matrix with basis functions $|S\uparrow\rangle$ and $|S\downarrow\rangle$. Its eigenvalue is written as

$$E_\mathrm{c}=E_\mathrm{s}+\frac{\hbar^2}{2m_\perp^e}\left(k_\mathrm{x}^2+k_\mathrm{y}^2\right)+\frac{\hbar^2}{2m_\parallel^e}k_\mathrm{z}^2+a_{\mathrm{c}1}\,\varepsilon_{zz}+a_{\mathrm{c}2}\,(\varepsilon_{xx}+\varepsilon_{yy}), \quad (6)$$

where $m_\parallel^e$ and $m_\perp^e$ denote the anisotropic effective masses of the electron parallel and perpendicular to the c-axis. $a_{\mathrm{c}1}$ and $a_{\mathrm{c}2}$ are conduction band deformation potentials along the c-axis and perpendicular to the c-axis, which can be related to the deformation potentials $D_{1,2}$ of the valence bands:

$$a_{\mathrm{c}1}=a_1+D_1, \quad a_{\mathrm{c}2}=a_2+D_2, \quad (7)$$

where $a_{1,2}$ describe the energetic shift of the total band gap with strain.

To set up the Hamiltonian for any growth orientation with an inclination angle θ with respect to the crystal c-axis, several quantities in the Hamiltonian have to be transformed to the growth coordinate system (x', y', z') using the transformation matrix $U(\varphi, \theta)$. Due to a radial symmetry of the wurtzite crystal in the c-plane, one expects an isotropic behavior in the c-plane, thus $\varphi = 0$, indicating that rotation around the x- and y-axes is equivalent. Therefore, it is sufficient to transform physical quantities only dependent on the inclination angle θ. This can be applied to the wave vectors as well,

$$\begin{pmatrix} k'_x \\ k'_y \\ k'_z \end{pmatrix} = \mathrm{U}(\theta) \begin{pmatrix} k_x \\ k_y \\ k_z \end{pmatrix} \tag{8}$$

with

$$\mathrm{U}(\theta) = \begin{pmatrix} \cos\theta & 0 & -\sin\theta \\ 0 & 1 & 0 \\ \sin\theta & 0 & \cos \end{pmatrix}. \tag{9}$$

In addition, to calculate the strain components of semipolar $(11\bar{2}2)$ AlInN/GaN layers, particularly for the shear strain (ε_{xz}) and the out-of-plane strain (ε_{zz}), the models described in Refs. [29,32] are used, respectively, with the parameter sets suggested by Vurgaftmann *et al.* [16]. As mentioned earlier, the large negative crystal-field splitting in AlN inverts the valence band order near the Γ point, thus the symmetry of the valence band states in AlInN is fundamentally different from GaN-based systems, which in turn could change the optical selection rules. Thus, it is essential to consider the VB structure of AlInN near the zone center ($k = 0$).

Figure 3(a) shows the VB structure for a biaxially strained AlInN/GaN on c-plane orientation. Due to the large negative crystal-field energy in AlN, the band character of the uppermost VB changes from Γ_9^V for the case of GaN [15] to Γ_{7-}^V in AlInN, followed by the Γ_9^V band and the Γ_7^V band in the order of increasing VB edge energy. Under biaxial compressive strain $\varepsilon_{xx} = \varepsilon_{yy} = -0.1\%$, the band dispersion exhibits an isotropic behavior in the k_x-k_y plane, i.e., the effective masses remain the same along the k_x- and k_y-directions. This suggests that the radial symmetry of the c-plane is preserved under isotropic in-plane strain. On the other hand, the semipolar $(11\bar{2}2)$ AlInN/GaN layer (sample S3) exhibits strongly anisotropic band dispersions in the $k_{c'}$-k_m plane, as shown in Fig. 3(b). The effective mass of the Γ_{7-}^V band along k_m remains nearly constant after changing the crystal orientation, but the effective mass along the $k_{c'}$-direction reduces significantly in the semipolar plane. For the Γ_9^V band, the effective masses reduce near the Γ point. In principle, the effective masses can be obtained from the calculated band structure by fitting the dispersion curves with a parabolic function. The obtained anisotropic effective masses along the k'_c- and k_m-directions for the two uppermost VBs are listed in Table II. The effective mass reflects the curvature of the band, and thus the optical transition near the Γ point could be directly influenced by the change of the band curvature with the k-vector, e.g., the crossing of bands near the vicinity of the Γ point. The effects of the effective mass on the optical transition can easily be taken into account by calculating the overlap integral of the wave functions of the electron in the conduction band and of the holes in the VBs, as will be

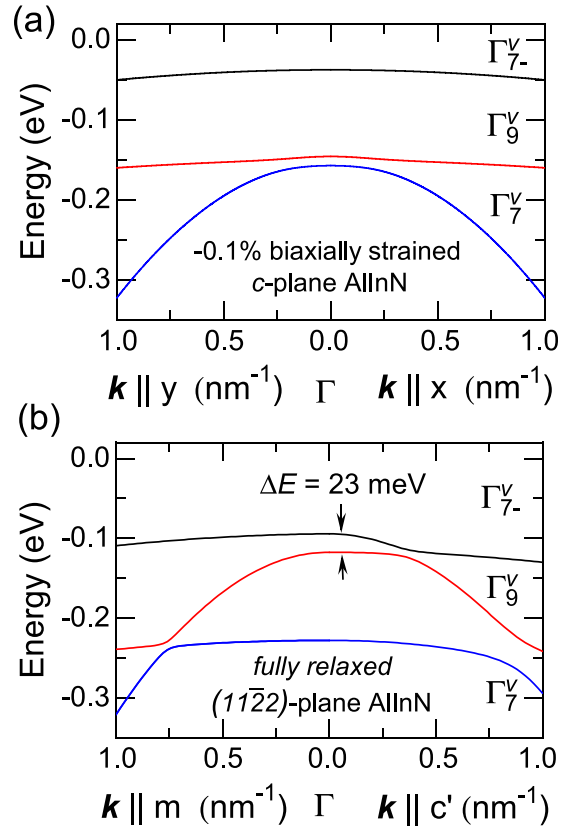

FIG. 3. The calculated valence band structures (a) for a c-plane AlInN/GaN layer under biaxial strain $\varepsilon_{xx} = \varepsilon_{yy} = -0.1\%$, and (b) for the $(11\bar{2}2)$ AlInN/GaN layer, sample S3. Due to the anisotropic in-plane strain as well as the reduced crystal symmetry in semipolar layers, the in-plane effective masses exhibit a strong anisotropy in the $k_{c'}$-k_m plane. The strain values for the band calculation are extracted from the XRD analysis, as listed in Table II. Note that the band gaps of AlN = 6.02 eV [33] and InN = 0.68 eV [34], as well as a bowing value of 6.0 eV [12], were used for the calculation.

TABLE II. Strain values extracted from the XRD analysis, the anisotropic hole effective masses for Γ_9^V and Γ_{7-}^V bands in units of m_0 in the $k_{c'}$-k_m plane, the band splitting $\Delta E_{\Gamma_{7-}-\Gamma_9}$ between these two bands at $k = 0$, as well as both the experimentally ($\rho_{\mathrm{Expt.}}$) and theoretically ($\rho_{\mathrm{Calc.}}$) estimated polarization degrees are listed.

Sample	S1	S2	S3
ε_{xx} (%)	−0.015	0.121	0.037
ε_{yy} (%)	−0.817	−0.904	−0.009
ε_{zz} (%)	−0.109	−0.005	−0.326
ε_{xz} (%)	0.3	0.2	−0.1
$m_{kc'}^{\Gamma_{7-}}$	0.22	0.22	0.22
$m_{km}^{\Gamma_{7-}}$	2.17	1.93	1.74
$m_{kc'}^{\Gamma_9}$	2.21	1.95	1.75
$m_{km}^{\Gamma_9}$	0.19	0.19	0.20
$\Delta E_{\Gamma_{7-}-\Gamma_9}$ (meV)	33.33	26.55	23.03
$\rho_{\mathrm{Expt.}}$	0.34 ± 0.01	0.25 ± 0.02	0.20 ± 0.01
$\rho_{\mathrm{Calc.}}$	0.61	0.57	0.42

discussed in the following. In addition, the model predicts a small energy splitting of 23 meV between the two uppermost VBs for sample S3, indicating a considerable hole occupation in the second Γ_9^V band at room temperature. This theoretically predicted value is consistent with the experimentally observed emission energy separation of around $\Delta E \approx 18 \pm 1$ meV between the two in-plane polarization directions, as shown in Fig. 2(a). Besides, a general trend of the decrease of the energy separation is observed with increasing strain relaxation along the m-direction for $(11\bar{2}2)$ AlInN/GaN layers, see Table II, suggesting that a reduction of the polarization degree can be expected with strain relaxation.

From the above discussions, it should be pointed out that the band crossing occurs between the valence Γ_{7-}^V band and the Γ_9^V band along the $k_{c'}$-direction with increasing of the k-vector in the semipolar plane, as evidenced from Fig. 3(b). It suggests that the band crossing in the vicinity of the zone center ($k = 0$) could result in the formation of new band states from mixing of the former VB basis functions defined for the c-plane case in Eq. (5). This is indeed a strong indication that the intermixing characteristics of the valence Γ_{7-}^V band and Γ_9^V band states between $|X\rangle$, $|Y\rangle$, $|Z\rangle$ orbital wave functions could be responsible for the polarized light emission from semipolar AlInN structures. Therefore, it becomes necessary to consider the wave-function overlap of those states to get some insight into the observed polarization anisotropy in semipolar $(11\bar{2}2)$ AlInN/GaN layers.

V. TRANSITION MATRIX ELEMENTS

The change in the band dispersion and thereby the effective mass has a direct impact on the optical transition matrix elements between the electron wave function and the hole wave function near the Γ point in the Brillouin zone. The general form of the optical transition matrix $|\mathbf{M}|^2$ between these states is given by [29]

$$|\hat{e}_i \mathbf{M}_i|^2 = |\langle \Psi_c | \hat{e}_i \mathbf{p} | \Psi_v \rangle|^2, \tag{10}$$

where $\hat{e}_i$ denotes a unit vector in different polarization directions in the growth coordinate, e.g., $i = x'$, y', z', and $\mathbf{p}$ represents the momentum operator. $|\Psi_c\rangle$ denotes the electron wave function in the CB, which has the symmetry of the atomic s-orbital wave function, while $|\Psi_v\rangle$ represents the hole wave functions in the VBs. Therefore, three matrix elements for each VB can be obtained, considering the spin-up and spin-down states. For semipolar orientation with $\theta = 58^\circ$, the in-plane transition matrix elements $|M_{[11\bar{2}\bar{3}]}|^2$ and $|M_{[1\bar{1}00]}|^2$, as well as the out-of-plane transition matrix elements $|M_{[11\bar{2}2]}|^2$, are given as follows [29]:

$$\begin{aligned} |M_{[11\bar{2}\bar{3}]}|^2 = & \left| -\frac{1}{\sqrt{2}}(b_{2v} - b_{1v})\cos(\theta)\langle S\uparrow | p_x | X\uparrow\rangle \right. \\ & \left. - b_{3v}\sin(\theta)\langle S\uparrow | p_z | Z\uparrow\rangle \right|^2 \\ & + \left| -\frac{1}{\sqrt{2}}(b_{5v} - b_{4v})\cos(\theta)\langle S\downarrow | p_x | X\downarrow\rangle \right. \\ & \left. - b_{6v}\sin(\theta)\langle S\downarrow | p_z | Z\downarrow\rangle \right|^2, \end{aligned} \tag{11}$$

$$\begin{aligned} |M_{[1\bar{1}00]}|^2 = & \left| \frac{1}{\sqrt{2}}(b_{1v} + b_{2v})\cos(\theta)\langle S\uparrow | p_y | Y\uparrow\rangle \right|^2 \\ & + \left| \frac{1}{\sqrt{2}}(b_{4v} + b_{5v})\cos(\theta)\langle S\downarrow | p_y | Y\downarrow\rangle \right|^2, \end{aligned} \tag{12}$$

and the out-of-plane transition matrix element ($\hat{e}_i = [11\bar{2}2]$)

$$\begin{aligned} |M_{[11\bar{2}2]}|^2 = & \left| -\frac{1}{\sqrt{2}}(b_{2v} - b_{1v})\sin(\theta)\langle S\uparrow | p_x | X\uparrow\rangle \right. \\ & \left. + b_{3v}\cos(\theta)\langle S\uparrow | p_z | Z\uparrow\rangle \right|^2 \\ & + \left| -\frac{1}{\sqrt{2}}(b_{5v} - b_{4v})\sin(\theta)\langle S\downarrow | p_x | X\downarrow\rangle \right. \\ & \left. + b_{6v}\cos(\theta)\langle S\downarrow | p_z | Z\downarrow\rangle \right|^2, \end{aligned} \tag{13}$$

where b_{iv} ($i = 1, 2, 3, \ldots, 6$) are the coefficients of the valence band wave functions $|\Psi_v\rangle$ defined in Eq. (5), and v ($v = \Gamma_{7-}^V$, Γ_9^V, and Γ_7^V) are the three valence bands in the case for AlInN. As the conduction band wave function $|\Psi_c\rangle$ has radial symmetry like the atomic s-orbital function, the anisotropic polarization properties are mostly determined by the hole states associated with $|X\rangle$, $|Y\rangle$, and $|Z\rangle$ orbital functions.

Figure 4 shows the obtained optical transition matrix elements as a function of the wave vector $k_{c'}$ for the $[11\bar{2}\bar{3}]$, $[1\bar{1}00]$, and $[11\bar{2}2]$ polarizations of semipolar $(11\bar{2}2)$ AlInN, sample S3. It is obvious that the optical matrix element for the C transition from the CB to the Γ_{7-}^V valence band is strongly polarized along the $[11\bar{2}\bar{3}]$ direction near the zone center ($k = 0$), as depicted in Fig. 4(a), but the contribution of the Γ_{7-}^V band for the $[11\bar{2}\bar{3}]$ polarization becomes less dominant with increasing wave vector, while the contribution from the Γ_9^V band starts to become significant. On the other hand, the optical matrix element between the Γ_9^V band and the CB states near the zone center indicates partial polarization along the $[1\bar{1}00]$ direction, as shown in Fig. 4(b). However, due to the intermixing of the states between the Γ_{7-}^V and Γ_9^V bands upon increasing the wave vector in the $k_{c'}$-direction, as shown in Fig. 3(b), the contribution of the Γ_{7-}^V band to the polarization along the $[1\bar{1}00]$ direction starts to come into play. Additionally, the lowest Γ_7^V band does not contribute to the polarization either in the $[11\bar{2}\bar{3}]$ or $[1\bar{1}00]$ direction, but the optical matrix element for the transition between the Γ_7^V band and the CB is strongly dominated by the polarization in the $[11\bar{2}2]$ direction, as shown in Fig. 4(c). Thus, we consider only the two uppermost Γ_{7-}^V and Γ_9^V bands in the following discussion. Further, to quantify the contribution of the transition matrix elements of the two uppermost VBs to the polarized PL emission in a certain direction, we need to consider the thermal distribution of carriers (holes) to the second VB Γ_9^V at room temperature since the energy difference between the Γ_{7-}^V and Γ_9^V bands is of the same order or lower than that of the typical thermal energy (≈26 meV); see Table II. These small energy separations cause larger hole occupation in the second uppermost band, which can be estimated using a Boltzmann distribution. This

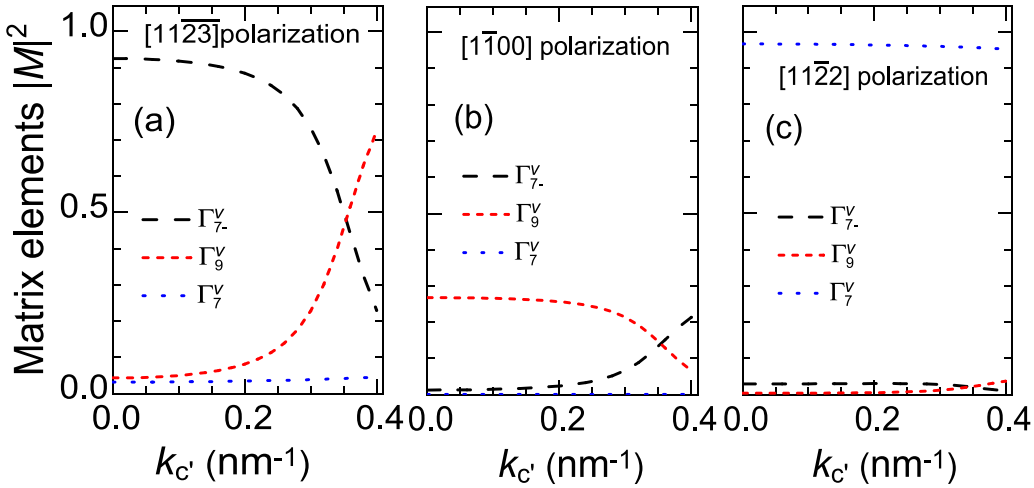

FIG. 4. k-dependent optical transition matrix elements at the band edges for the (a) [11$\bar{2}\bar{3}$], (b) [1$\bar{1}$00], and (c) [11$\bar{2}$2] polarizations of the semipolar (11$\bar{2}$2) AlInN (sample S3).

can be applied because the PL measurements are conducted under a low-excitation power regime, i.e., the nondegenerate limit where the quasi-Fermi-level lies far above the VB edge. Therefore, it is sufficient to take the relative energy difference between the valence Γ_{7-}^V and Γ_9^V bands to estimate the thermal occupation of the valence Γ_9^V band as follows:

$$\frac{f_{\Gamma_9}}{f_{\Gamma_{7-}}} = \exp\left(-\frac{\Delta E_{\Gamma_{7-}-\Gamma_9}}{k_B T}\right), \tag{14}$$

where $\Delta E_{\Gamma_{7-}-\Gamma_9}$ represents the energy separation between the two uppermost valence bands. For example, an energy splitting of 23 meV at the zone center ($k = 0$) results in a sizable population of $f_{\Gamma_9}/f_{\Gamma_{7-}} = 41\%$ of the Γ_9^V band for the sample S3. As seen earlier in Fig. 3(b), the energy difference becomes smaller upon increasing the wave vector in the direction where the band crossing occurs, which results in an even higher population. Consequently, these occupied states will contribute to light emission in both in-plane directions. Therefore, the effective degree of polarization can be estimated by combining the transition matrix elements together with the thermal occupation of the Γ_9^V band.

The polarization degree of the transition matrix elements is obtained by the two in-plane transition matrix elements $|M_{[11\bar{2}\bar{3}]}|^2$ and $|M_{[1\bar{1}00]}|^2$ as follows [35]:

$$\rho_{\mathrm{m}} = \frac{|M_{[11\bar{2}\bar{3}]}|^2 - |M_{[1\bar{1}00]}|^2}{|M_{[11\bar{2}\bar{3}]}|^2 + |M_{[1\bar{1}00]}|^2}, \tag{15}$$

where $\rho_{\mathrm{m}} = 1$ can be expected for total [11$\bar{2}\bar{3}$] polarization when the [1$\bar{1}$00] polarization completely vanishes. But we expect to see partial polarization of the transitions for semipolar (11$\bar{2}$2) AlInN, since both band to band transitions from the valence Γ_{7-}^V and Γ_9^V bands to the CB can contribute to the polarization either along the [11$\bar{2}\bar{3}$] direction or along the [1$\bar{1}$00] direction. Each matrix element in Eq. (15) represents the sum of the transition matrix elements associated with the two uppermost VBs for a given polarization direction due to the band crossing, as discussed previously. Again, to correlate the calculated transition matrix elements together with the thermal population of the second VB Γ_9^V to the measured PL intensity (I_{PL}), i.e., $I_{\mathrm{PL}} \propto f_{\Gamma_9^V}/f_{\Gamma_{7-}^V}\,|M_i|^2$, one needs to consider all possible transitions in k-space and integrate over all directions, according to Fermi's golden rule. For this, transition matrix elements are calculated for the two orthogonal directions for the k-vector maximum up to 1.5/ nm in the $k_{c'}$-k_{m} plane, and they are averaged over in the $k_{c'}$-k_{m} plane [36]. It is worth mentioning that the choice of such a high k-value here is not arbitrary, but it is a meaningful maximum k-value for states occupied by carriers when we take the energy range up to around $2k_BT$ from the zone center. Interestingly enough, the theoretical model predicts a polarization ratio ρ_{m} of 0.42 for sample S3, which is somewhat higher than the measured effective polarization ratio $\rho = 0.20 \pm 0.01$ at room temperature; see Table II. Of course, there are several possible aspects that need to be considered to explain the discrepancy between the model prediction and the experiment.

The band parameters, especially the deformation potentials D_1–D_6, are obtained by a linear interpolation between the corresponding values of AlN and InN for the given indium composition. The deformation potentials D_5 and D_6, which are associated with the off-diagonal entries of the VB matrix in Eq. (2), have a direct influence on the VB splittings of semipolar (11$\bar{2}$2) structure through anisotropic strain (D_5) and shear strain (D_6) [27]. According to Ref. [16], the values of $D_6 = -3.4$ eV for AlN and $D_6 = -5.5$ eV for InN were derived from another existing deformation potential using the quasicubic approximation and not from the experiment. Furthermore, it is likely that it is challenging to accurately determine those values from the experiment due to the fact that most of the investigated samples in the literature were grown on c-plane structures where isotropic and shear strain components become zero. Ultimately, this could lead to a lack of accurate band parameter sets, as several available parameter sets in the literature are mainly obtained from theoretical calculations [37,38]. Also, the difficulty in growing high-quality InN makes the determination of the band parameters for InN a persistent problem. In addition, the anisotropic strain components ε_{xx}, ε_{yy}, ε_{zz} as well as the shear component ε_{xz} for semipolar (11$\bar{2}$2) AlInN layers are directly determined from the XRD analysis; see Table II. However, as demonstrated in

Ref. [6], semipolar $(11\bar{2}2)$ AlInN layers do not have well-defined strain states, e.g., the upper part of the layers exhibits partial relaxation along the *m*-direction while the lower part of the AlInN layer is grown pseudomorphically on GaN. It is also shown that the thickness of the relaxed part depends on the thickness of the AlInN, and the strain relaxation takes place in a thickness of about 140 nm for the 400-nm-thick AlInN (sample S3). For the strained part, the strain values can be determined within some accuracy, but the relaxed part can only be determined by estimated values from the reciprocal space maps, which come with large uncertainties. Thus, the mixture of strain states in the AlInN layers close to the surface makes it more challenging to evaluate more reliable strain values. Therefore, the inconsistent band parameter sets of AlN and InN as well as the large uncertainty in the strain values of semipolar $(11\bar{2}2)$ AlInN layers are likely responsible for the difference in the absolute values of the polarization degrees obtained experimentally and theoretically.

After all, it is worthwhile to point out that the model calculation predicts very well the dependence of the polarization degree on strain relaxation, as discussed in Sec. III. The absolute values of the polarization degree (ρ_m) are not in perfect agreement with the experimental values (ρ). From the model, polarization degrees of 0.61 and 0.57 are obtained for samples S1 and S2, corresponding to strain relaxation degrees of $31 \pm 2\%$ and $39 \pm 10\%$ in the *m*-direction, respectively; see Table II. The observed dependence of the polarization ratio on strain relaxation is indeed confirmed by the current model, supporting earlier theoretical predictions as well [27,29].

VI. TRANSITION ENERGY AND LARGE STOKES SHIFT

The bowing parameter *b* describes a nonlinear dependence of the band gap on composition in semiconductor alloys. As a result, it becomes essential to know a reliable bowing value to determine the variation of the band gap with indium mole fraction. However, the bowing values of $Al_{1-x}In_xN$ reported in the literature vary strongly, which could be due to several reasons, as mentioned in the Introduction. The literature values of the band gap as well as bowing parameters are summarized in Fig. 5. Sakalauskas *et al.* [9] have reported a composition-dependent bowing of 5.36 eV extracted from the band-edge absorption for MOVPE-grown $Al_{1-x}In_xN$ layers with indium composition between 0.143 and 0.242. In contrast, Aschenbrenner *et al.* [14] have reported a large bowing parameter of 10.3 eV for $Al_{1-x}In_xN$ films grown on *c*-plane sapphire using MOVPE. Besides, Wang *et al.* [12] have studied *c*-plane $Al_{1-x}In_xN$ epilayers with indium content ranging from 0.13 to 0.24 using both PL and PL excitation spectroscopies. A bowing parameter of about 6 eV is derived from the indium composition dependencies of PL emission and absorption. Interestingly, large Stokes shifts between 0.4 and 0.8 eV are observed between luminescence emissions and absorption edges. Thus, it can be concluded that we cannot completely exclude the effects of the different growth methods on the crystalline quality of AlInN layers, which in turn could give rise to slight differences in the emission energy due to different strain status in the layers, e.g., the strain-related shift of the band. But this could not be of significant importance when we compare the optical properties of AlInN

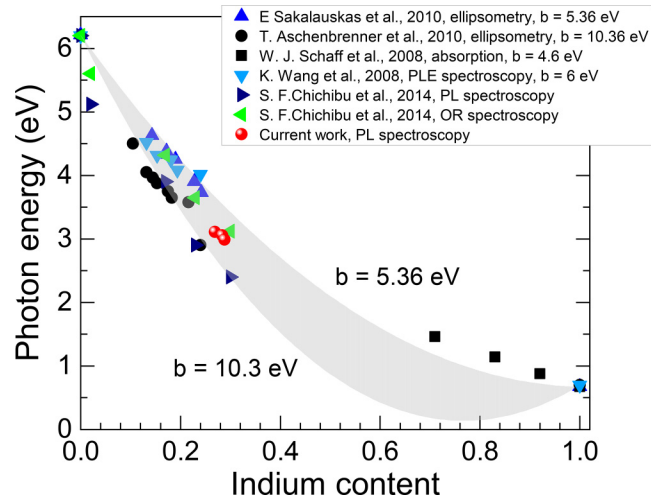

FIG. 5. The experimental dependence of the band gap of $Al_{1-x}In_xN$ on indium composition *x*. The reported values of the band gap and the bowing parameter *b* are depicted. The two fit curves with bowing values of 5.36 eV [9] and 10.3 eV [14] are plotted using an empirical expression as $E_g(x) = (1-x)E_g(\mathrm{AlN}) + xE_g(\mathrm{InN}) - bx(1-x)$. The area between them is filled with color. In addition, the band gaps of AlN = 6.02 eV [33] and InN = 0.68 eV [34] are used for reproducing the fit curves.

layers grown under the same conditions but characterized with different optical techniques. For example, a large Stokes shift of ~ 0.6 eV in Ref. [12] is not likely due to strain, but rather the interband transition matrix elements, which in turn obey the polarization selection rules arising from the VB ordering near the Γ point ($k = 0$) for AlInN. From the study of the polarization properties of semipolar $(11\bar{2}2)$ AlInN, we found that AlInN possesses a valence band ordering similar to AlN, where the C interband transition is allowed for an electric field parallel to the *c*-axis ($E \parallel c$) but strictly forbidden for polarization perpendicular to the *c*-axis ($E \perp c$), whereas the interband transitions from the valence Γ_9^V and Γ_7^V bands to the CB are only allowed for an electric field perpendicular to the *c*-axis ($E \perp c$), as depicted in Fig. 6.

To link the strong variation of the band gap of AlInN with the observed optical selection rules, the indium composition dependence of the interband transition energies at the Brillouin zone center ($k = 0$) between the lowest CB edge and

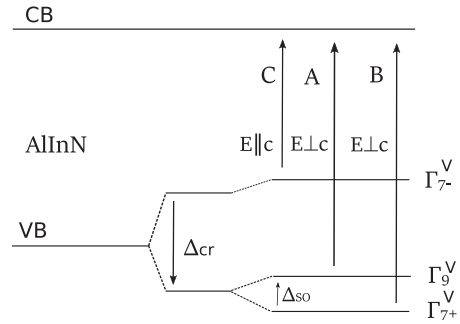

FIG. 6. Schematic representation of the valence band structure and the polarization selection rules for AlInN.

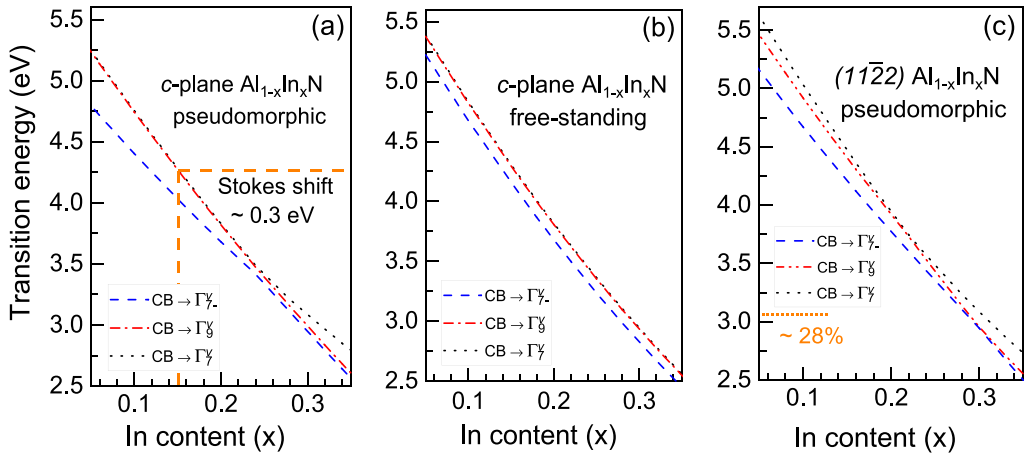

FIG. 7. Calculated interband transition energies at $k = 0$ between the lowest CB and the three uppermost Γ_{7-}^{V}, Γ_{9}^{V}, and Γ_{7}^{V} bands in order of increasing transition energy for pseudomorphically grown c-plane AlInN (a), free-standing c-plane AlInN (b), and pseudomorphically grown semipolar (11$\bar{2}$2) AlInN (c) as a function of indium composition at 300 K. Also, a Stokes shift of about 0.2 eV for the lattice-matched case (18%) is indicated (a), and the calculated transition energy of around 3.1 eV at an indium composition of about 28% is marked for coherently grown semipolar (11$\bar{2}$2) AlInN (c), indicating the calculated value is consistent with the measured PL emission for the samples under consideration, as shown in Fig. 1.

the three uppermost Γ_{7-}^{V}, Γ_{9}^{V}, and Γ_{7}^{V} bands is calculated as follows [39]:

$$E_i = E_s + E_{\mathrm{cb}} - E_j^{\mathrm{vb}} - E_{\mathrm{ex}}, \tag{16}$$

where E_s is given as

$$E_{\mathrm{s}} = E_{\mathrm{g}} + \Delta_{\mathrm{cr}} + \frac{\Delta_{\mathrm{so}}}{3}, \tag{17}$$

where E_{g}, Δ_{cr}, and Δ_{so} are the composition-dependent band gap, crystal-field splitting, and spin-orbit splitting of AlInN, which are linearly interpolated between the corresponding values of AlN and InN, given in Refs. [16,33,34]. E_{cb} denotes the CB energy introduced in Eq. (6). $E_{\mathrm{j}}^{\mathrm{vb}}$ represents the VB edge energies of the three uppermost valence bands at $k = 0$. E_{ex} denotes the composition dependent exciton binding energy, and it is linearly interpolated between the values of 51 meV [33] and 3 meV [34] for AlN and InN, respectively, for all the transitions.

Figure 7(a) shows the change of the calculated transition energies E_{i} as a function of indium composition for pseudomorphically grown AlInN on c-plane GaN. The interband transition C from the lowest CB to the uppermost valence Γ_{7-}^{V} band (dashed blue) spans an emission energy from about 4.6–2.8 eV for the given indium content up to $x = 0.35$. The transition energies of the CB to the second and third VBs are almost overlapped up to an indium composition of about 25%, and then there occurs a crossing of bands between the valence Γ_{7-}^{V} and Γ_{7}^{V} bands due to the change of band characters with strain. As mentioned earlier, the interband transition C is only allowed for the polarization parallel to the c-axis ($E \parallel c$). This provides strong evidence that this transition, which determines the fundamental band gap for c-plane AlInN, is hardly detectable for optical characterization with light normal to the c-plane for c-plane structures such as absorption, transmission, and reflectance measurements, whereas the luminescence can be observable, which most likely stems from light scattered from the interband transition C between the CB and the uppermost Γ_{7-}^{V} band. On the other hand, the band to band A and B transitions are allowed for the polarization perpendicular to the c-axis ($E \perp c$), which should be easily detectable by optical measurements with light incidence normal to the sample surface. As a result, the large variation in the band gap and thereby the bowing parameters, as well as the large Stokes shift, seem to originate from the lack of clarity regarding the optical selection rules for c-plane AlInN. For example, Wang *et al.* [12] observed a large Stokes shift of around 0.4 eV between the luminescence and absorption edge for a c-plane AlInN layer with an indium content of 15.3%. As can be seen in Fig. 7(a), the energy difference between the interband transitions C and A (or B) amounts to about 0.3 eV for the case of 15% and 0.2 eV for the lattice-matched (18%) case, which is closer to the 0.4 eV found experimentally (15.3%) [12]. Of course, the absolute value of the Stokes shift in the calculation depends strongly on the choice of the band parameters as well, as discussed in the previous section. Additionally, localization of the excitons at certain potential minima due to inhomogeneity is considered as an additional cause of the Stokes shift in AlInN layers [12,13,40].

Figure 7(b) shows the three interband transition energies for c-plane AlInN under full relaxation. From the parallel decreases of the energies of the transitions C and A (or B) with increasing indium composition, it can be concluded that the band order of AlInN is preserved for a wide range of compositions, thereby providing strong evidence that strain plays a significant rule in band mixing and consequently polarization switching. Further, Fig. 7(c) depicts the three transition energies for the case of pseudomorphically grown semipolar (11$\bar{2}$2) AlInN. Unlike polar c-plane structures, semipolar structures exhibit an optical polarization anisotropy due to the reduced crystal symmetry as well as anisotropic in-plane strain. This is indeed confirmed by both the experiment and theoretical model in the previous sections. There, the C transition from the topmost Γ_{7-}^{V} band to the CB is strongly polarized

along the $[11\bar{2}\bar{3}]$ ($E \parallel c'$), whereas the Γ_9^V band shows a dominant polarization along the m-direction ($E \perp c'$), as shown in Fig. 4. In principle, an additional weakening of the strict optical selection rules can be expected for the case of a semipolar plane, since the projection of the crystal c-axis lies in the semipolar growth plane. As a result, it could be possible to detect the polarized light emission in either in-plane directions by using absorption (reflectance) or PL measurements for semipolar AlInN. As can be seen in Fig. 4(c), the calculated transition energy of around 3.1 eV between the valence Γ_{7-}^V band and the CB at $k = 0$ with indium composition of about 28% is in agreement with the measured PL emission energy of ≈3.1 eV for samples (S1, S2, and S3); see Fig. 1. Nonetheless, to confirm the results regarding the polarization selection rules for AlInN presented in this work, further optical measurements such as absorption (reflectance) need to be performed to examine the polarization properties of semipolar AlInN, and the results should be compared with those obtained with PL measurements.

VII. CONCLUSIONS

The valence band ordering in AlInN is investigated by studying the optical polarization anisotropy of semipolar $(11\bar{2}2)$ AlInN/GaN layers. On the one hand, the polarization resolved PL measurements reveal a strong polarization along the $[11\bar{2}\bar{3}]$ direction and a weaker signal along the $[1\bar{1}00]$ direction in the $(11\bar{2}2)$ plane. The polarization degree is found to be dependent on strain relaxation along the $[1\bar{1}00]$ direction, where a decrease of the polarization degree is observed with increasing strain relaxation. On the other hand, the $\mathbf{k} \cdot \mathbf{p}$ approach was employed to evaluate the optical properties (e.g., the band dispersion, transition matrix, and transition energy) of AlInN near the zone center ($k = 0$). Interestingly, AlInN exhibits a valence band ordering similar to AlN due to the large negative crystal-field splitting, where the uppermost VB is Γ_{7-}^V, following by the Γ_9^V and Γ_7^V bands. Further, the in-plane transition matrix elements from the CB to the two uppermost bands near the Γ point are dominated by $M_{[11\bar{2}\bar{3}]}$ for the Γ_{7-}^V band and by $M_{[1\bar{1}00]}$ for the Γ_9^V band. By combining the transition matrix elements together with the thermal occupation of the second uppermost Γ_9^V band, reasonable agreement between the experiment and the model is obtained in regard to both the polarization degree and the strain-dependent polarization, indicating the reliability of the model. Furthermore, the obtained polarization selection rules are used to explain the large variation of the band gap and the strong Stokes shift observed previously in AlInN [9–14] by calculating the transition energy, suggesting that the lack of clarity regarding the polarization selection rules is more likely responsible for the large scattering of the band-gap values.

The data that support the findings of this study are available from the corresponding author upon reasonable request.

ACKNOWLEDGMENTS

S.S. gratefully acknowledges the financial support from the NTH School for Contacts in Nanosystems at the early stage of this work, and the support by the Braunschweig International Graduate School of Metrology (B-IGSM).

[1] D. S. Lee, J. W. Chung, H. Wang, X. Gao, S. Guo, P. Fay, and T. Palacios, 245-GHz InAlN/GaN HEMTs with oxygen plasma treatment, IEEE Electron Dev. Lett. **32**, 755 (2011).

[2] M. Mikulics, R. Stoklas, A. Dadgar, D. Gregušová, J. Novák, D. Grützmacher, A. Krost, and P. Kordoš, InAlN/GaN/Si heterostructures and field-effect transistors with lattice matched and tensely or compressively strained InAlN, Appl. Phys. Lett. **97**, 173505 (2010).

[3] R. Butté, J.-F. Carlin, E. Feltin, M. Gonschorek, S. Nicolay, G. Christmann, D. Simeonov, A. Castiglia, J. Dorsaz, H. J. Buehlmann, S. Christopoulos, G. B. H. von Hög, A. J. D. Grundy, M. Mosca, C. Pinquier, M. A. Py, F. Demangeot, J. Frandon, P. G. Lagoudakis, J. J. Baumberg *et al.*, Current status of AlInN layers lattice-matched to GaN for photonics and electronics, J. Phys. D **40**, 6328 (2007).

[4] H. P. D. Schenk, M. Nemoz, M. Korytov, P. Vennéguès, A. D. Dräger, and A. Hangleiter, Indium incorporation dynamics into AlInN ternary alloys for laser structures lattice matched to GaN, Appl. Phys. Lett. **93**, 081116 (2008).

[5] L. Vegard, Die Konstitution der Mischkristalle und die Raumfüllung der Atome, Z. Phys. **5**, 17 (1921).

[6] E. R. Buß, P. Horenburg, U. Rossow, H. Bremers, T. Meisch, M. Caliebe, F. Scholz, and A. Hangleiter, Non- and semipolar AlInN one-dimensionally lattice-matched to GaN for realization of relaxed buffer layers for strain engineering in optically active GaN-based devices, Phys. Status Solidi B **253**, 84 (2016).

[7] E. R. Buß, U. Rossow, H. Bremers, T. Meisch, M. Caliebe, F. Scholz, and A. Hangleiter, Intentional anisotropic strain relaxation in $(11\bar{2}2)$ oriented $Al_{1-x}In_xN$ one-dimensionally lattice matched to GaN, Appl. Phys. Lett. **105**, 122109 (2014).

[8] P. Henning, P. Horenburg, H. Bremers, U. Rossow, F. Tendille, P. Vennégués, P. de Mierry, J. Zúñiga-Pérez, and A. Hangleiter, Reduced nonradiative recombination in semipolar green-emitting III-N quantum wells with strain-reducing AlInN buffer layers, Appl. Phys. Lett. **115**, 202103 (2019).

[9] R. Goldhahn, P. Schley, A. T. Winzer, G. Gobsch, V. Cimalla, O. Ambacher, M. Rakel, C. Cobet, N. Esser, H. Lu, and W. J. Schaff, Detailed analysis of the dielectric function for wurtzite InN and In-rich InAlN alloys, Phys. Status Solidi A **203**, 42 (2006).

[10] R. E. Jones, R. Broesler, K. M. Yu, J. W. Ager, E. E. Haller, W. Walukiewicz, X. Chen, and W. J. Schaff, Band gap bowing parameter of $In_{1-x}Al_xN$, J. Appl. Phys. **104**, 123501 (2008).

[11] J.-F. Carlin, C. Zellweger, J. Dorsaz, S. Nicolay, G. Christmann, E. Feltin, R. Butté, and N. Grandjean, Progresses in III-nitride distributed bragg reflectors and microcavities using AlInN/GaN materials, Phys. Status Solidi B **242**, 2326 (2005).

[12] K. Wang, R. W. Martin, E. Nogales, P. R. Edwards, K. P. O'Donnell, K. Lorenz, E. Alves, and I. M. Watson, Cathodo-

luminescence of rare earth implanted AlInN, Appl. Phys. Lett. **89**, 131912 (2006).

[13] S. F. Chichibu, K. Hazu, K. Furusawa, Y. Ishikawa, T. Onuma, T. Ohtomo, H. Ikeda, and K. Fujito, High internal quantum efficiency ultraviolet to green luminescence peaks from pseudomorphic *m*-plane $Al_{1-x}In_xN$ epilayers grown on a low defect density *m*-plane freestanding GaN substrate, J. Appl. Phys. **116**, 213501 (2014).

[14] T. Aschenbrenner, H. Dartsch, C. Kruse, M. Anastasescu, M. Stoica, M. Gartner, A. Pretorius, A. Rosenauer, T. Wagner, and D. Hommel, Optical and structural characterization of AlInN layers for optoelectronic applications, J. Appl. Phys. **108**, 063533 (2010).

[15] S. Wei and A. Zunger, Valence band splittings and band offsets of AlN, GaN, and InN, Appl. Phys. Lett. **69**, 2719 (1996).

[16] I. Vurgaftman and J. R. Meyer, Band parameters for nitrogen-containing semiconductors, J. Appl. Phys. **94**, 3675 (2003).

[17] R. Dingle, D. D. Sell, S. E. Stokowski, and M. Ilegems, Absorption, reflectance, and luminescence of GaN epitaxial layers, Phys. Rev. B **4**, 1211 (1971).

[18] M. Suzuki, T. Uenoyama, and A. Yanase, First-principles calculations of effective-mass parameters of AlN and GaN, Phys. Rev. B **52**, 8132 (1995).

[19] A. Rubio, J. L. Corkill, M. L. Cohen, E. L. Shirley, and S. G. Louie, Quasiparticle band structure of AlN and GaN, Phys. Rev. B **48**, 11810 (1993).

[20] M. R. Laskar, T. Ganguli, A. A. Rahman, A. Arora, N. Hatui, M. R. Gokhale, S. Ghosh, and A. Bhattacharya, Anisotropic structural and optical properties of *a*-plane $(11\bar{2}0)$ AlInN nearly-lattice-matched to GaN, Appl. Phys. Lett. **98**, 181108 (2011).

[21] S. Schwaiger, S. Metzner, T. Wunderer, I. Argut, J. Thalmair, F. Lipski, M. Wieneke, J. Bläsing, F. Bertram, J. Zweck, A. Krost, J. Christen, and F. Scholz, Growth and coalescence behavior of semipolar $(11\bar{2}2)$ GaN on pre-structured r-plane sapphire substrates, Phys. Status Solidi B **248**, 588 (2011).

[22] Due to the distortion in vacuum window during the processing, it has the stress-induced birefringence property with a radial symmetry. The fast (or slow) axis is positioned along the radial axis and thus differs from point to point. In the center, however, the effect of the curvature is not significant, and the tangential plane is a good approximation. Thus we expect a minimum ellipticity in the polarization of the emitted light caused by the stress acting on the window. Outside of the center this effect will become significant, and this could have a large impact on the polarization degree. To avoid a distortion of the polarized PL signal during the measurements, it is important to adjust the sample position to the center of vacuum window.

[23] M. Ueda, K. Kojima, M. Funato, Y. Kawakami, Y. Narukawa, and T. Mukai, Epitaxial growth and optical properties of semipolar $(11\bar{2}2)$ GaN and InGaN/GaN quantum wells on GaN bulk substrates, Appl. Phys. Lett. **89**, 211907 (2006).

[24] L. Schade, U. T. Schwarz, T. Wernicke, M. Weyers, and M. Kneissl, Impact of band structure and transition matrix elements on polarization properties of the photoluminescence of semipolar and nonpolar InGaN quantum wells, Phys. Status Solidi B **248**, 638 (2011).

[25] M. Ueda, M. Funato, K. Kojima, Y. Kawakami, Y. Narukawa, and T. Mukai, Polarization switching phenomena in semipolar quantum well $In_xGa_{1-x}N$/GaN active layers, Phys. Rev. B **78**, 233303 (2008).

[26] A. A. Yamaguchi, Anisotropic optical matrix elements in strained GaN quantum wells on semipolar and nonpolar substrates, Jpn. J. Appl. Phys. **46**, L789 (2007).

[27] Q. Yan, P. Rinke, M. Scheffler, and C. G. Van de Walle, Role of strain in polarization switching in semipolar InGaN/GaN quantum wells, Appl. Phys. Lett. **97**, 181102 (2010).

[28] D. H. Goldstein, *Polarized Light*, 3rd ed. (CRC, Boca Raton, FL, 2011).

[29] S.-H. Park and S.-L. Chuang, Crystal-orientation effects on the piezoelectric field and electronic properties of strained wurtzite semiconductors, Phys. Rev. B **59**, 4725 (1999).

[30] S.-H. Park, D. Mishra, Y. Eugene Pak, C. Young Park, S.-H. Yoo, Y.-H. Cho, M.-B. Shim, S. Hwang, and S. Kim, Partial strain relaxation effects on polarization anisotropy of semipolar $(11\bar{2}2)$ InGaN/GaN quantum well structures, Appl. Phys. Lett. **103**, 221108 (2013).

[31] G. Bir and G. Pikus, *Symmetry and Strain-induced Effects in Semiconductors*, A Halsted Press book (Wiley, New York, 1974).

[32] H. Jönen, H. Bremers, U. Rossow, T. Langer, A. Kruse, L. Hoffmann, J. Thalmair, J. Zweck, S. Schwaiger, F. Scholz, and A. Hangleiter, Analysis of indium incorporation in non- and semipolar GaInN QW structures: Comparing x-ray diffraction and optical properties, Semicond. Sci. Technol. **27**, 024013 (2012).

[33] L. Chen, B. J. Skromme, R. F. Dalmau, R. Schlesser, Z. Sitar, C. Chen, W. Sun, J. Yang, M. A. Khan, M. L. Nakarmi, J. Y. Lin, and H.-X. Jiang, Band-edge exciton states in AlN single crystals and epitaxial layers, Appl. Phys. Lett. **85**, 4334 (2004).

[34] B. Monemar, P. Paskov, and A. Kasic, Optical properties of InN—the bandgap question, Superlattices Microstruct. **38**, 38 (2005).

[35] K. Kojima, H. Kamon, M. Funato, and Y. Kawakami, Theoretical investigations on anisotropic optical properties in semipolar and nonpolar InGaN quantum wells, Phys. Status Solidi C **5**, 3038 (2008).

[36] D. A. S. H. Park and S. L. Chuang, Electronic and optical properties of a- and m-plane wurtzite InGaN–GaN quantum wells, IEEE J. Quantum Electron. **43**, 1175 (2007).

[37] P. Rinke, M. Winkelnkemper, A. Qteish, D. Bimberg, J. Neugebauer, and M. Scheffler, Consistent set of band parameters for the group-III nitrides AlN, GaN, and InN, Phys. Rev. B **77**, 075202 (2008).

[38] Q. Yan, P. Rinke, M. Scheffler, and C. G. Van de Walle, Strain effects in group-III nitrides: Deformation potentials for AlN, GaN, and InN, Appl. Phys. Lett. **95**, 121111 (2009).

[39] S. Ghosh, P. Waltereit, O. Brandt, H. T. Grahn, and K. H. Ploog, Electronic band structure of wurtzite GaN under biaxial strain in the M plane investigated with photoreflectance spectroscopy, Phys. Rev. B **65**, 075202 (2002).

[40] T. Onuma, S. Chichibu, Y. Uchinuma, T. Sota, S. Yamaguchi, S. Kamiyama, H. Amano, and I. Akasaki, Recombination dynamics of localized excitons in $Al_{1-x}In_xN$ epitaxial films on GaN templates grown by metalorganic vapor phase epitaxy, J. Appl. Phys. **94**, 2449 (2003).